Custom imager as wavefront sensor

By: Davies W. de Lima Monteiro and Gleb Vdovin
Electronic Instrumentation Laboratory – ITS / Delft University of Technology
Mekelweg 4, 2628 CD Delft, The Netherlands (davies@ei.et.tudelft.nl)

Abstract

We report on an integrated Hartmann wavefront sensor (WFS) using passive-pixel architecture and pixels clustered as position-sensitive detectors for dynamic wavefront analysis. Such a device detects the degrees of imperfection (aberrations) of a light beam by measuring the deviation of the incoming wavefront from a reference one. It can be employed either as a diagnostic tool, or in close loop with a wavefront corrector in an Adaptive Optics (AO) system. AO deals with sensing and correcting distortions occurring in optical systems.
Keywords: *wavefront sensor, Adaptive Optics, CMOS imager.*

I. Introduction

As a diagnostic tool the wavefront sensor (WFS) can be used, for instance, in optical shop testing, analysis of fluid dynamics and ophtalmology to detect aberrations on the eye cornea [1,2,3]. When part of a close-loop AO system, it is coupled to an adaptive mirror to improve the quality of a light beam (Figure 1). The WFS then measures the distortions caused by the propagation media and the adaptive mirror adjusts its reflective surface to correct them. As a matter of fact, an image propagating through the same path as the beam can be corrected too. This is very useful in astronomical imaging, satellite optical communications and retinal imaging, for example. Dynamic correction at rates higher than 100Hz are demanded in several potential AO applications.

II. Hartmann wavefront sensor

Among several techniques to measure wavefront aberrations, we employ the Hartmann method for it be conceptually simple, capable of real-time analysis and suitable to both open- and close-loop operation. The method is based on having a wavefront sampled by an opaque mask with holes (Hartmann mask). It results in spots at the detector plane, as illustrated in Figure 2.
When the wavefront is flat, the spot centroids are all equally spaced. In contrast, when aberration is introduced, the spots are displaced from the initial positions. Each spot displacement is proportional to the local tilt present at the corresponding site. Thus, it is possible to obtain the deviation of a test wavefront from a reference one if the spot displacements are known. The estimation of the wavefront is done by using the modal reconstruction, where a vector of x and y displacements of all spots is decomposed over an orthogonal basis, built as a matrix of derivatives of known circular polynomials. It results in a wavefront spatial function $W(\rho,\phi)$ as given in Equation 1.

$$W(\rho,\phi) = \sum_{i=0}^{\max\_order} C_i P_i(\rho,\phi) \quad (1)$$

Where the index i runs up to the maximum order chosen for a particular application and each coefficient C_i determines the amount of the respective polynomial contributing to the wavefront aberration. Low-order terms relate to known aberrations as tilts, defocus, astigmatism and spherical aberration, whereas high-order ones represent distortions with higher spatial frequency. Usually 25 sampling spots provide sufficient data for accurate detection of low-order aberrations. As the number of spots increases, high-order aberration detection becomes more precise, at the expense of data handling time both for position tracking and for wavefront reconstruction.
To sum it up, our wavefront sensor has basically two main elements: a sampling plane and a multi-spot position detector. The first splits the wavefront into several sub-regions, whose phase information will be given by the position of spots. The latter detects all these positions, therefore providing the necessary data to estimate the wavefront shape.

III. Custom imager as multi-spot position detector

When one thinks of a video imager the initial issues of concern as regards its performance are typically three: resolution, sensitivity and frame rate. Image resolution is related to the number of pixels in a certain chip die. Sensitivity depends on the fill-factor, technology used and embedded circuitry. Frame rate is both dependent on the previous factors, the target image and the image

software. If affordability and compactness are added as desirable features it is unlikely they will be altogether optimized on a single device. Therefore, a trade-off among all these items will prove necessary for each particular application.

In the case of a Hartmann sensor, the multi-spot detector can in principle be a conventional charge-coupled device (CCD) or a CMOS imager, however neither of them allows fast enough frame readouts, unless expensive specialized CCD's are meant. Furthermore, both provide image outputs that must be further processed to find the spots centroids. In fact, simplifications on an imager will prove very efficient for this particular sensor.

Once a relatively small number of spots guarantees the detection of aberrations present in most optical systems of interest, and since position of each spot - rather than intensity distribution - is the required parameter, image resolution can be exchanged for direct position sensing. For this purpose several pixel clustering architectures have been studied [4], among which the simplest and with the highest sensitivity is the quad-cell (QC) layout. It has a very well defined center, offers high fill-factor and is not dependent on a resistive network. Each QC measures the position of one spot by simple mathematical calculations on the quad-cell signals, as suggested by Equations 2 and 3. The QC responses to spot displacements on x and y directions are given by x_{QC} and y_{QC}, which are normalized functions of the signals S_j, where j represents photodiode A, B, C or D (Figure 3).

$$x_{QC} = \frac{(S_B + S_C) - (S_A + S_D)}{S_j} \tag{2}$$

$$y_{QC} = \frac{(S_A + S_B) - (S_C + S_D)}{S_j} \tag{3}$$

A four-channel parallel output, rather than a serial output, enables all four pixels of a QC to be addressed simultaneously, thus avoiding that temporal artifacts influence the position information. This contributes to faster frame readout as well. Then, instead of row and column decoders, as usual for imagers, it is more convenient to have a customized decoder to access each quad-cell at a turn.

Silicon CMOS technology offers a good deal for compactness and affordability by enabling both digital and analog electronic circuitry to be integrated on the chip and by being widely available. State-of-the-art processes allow a very large amount of pixels and high circuit density, but have drawbacks for imaging as high stacks of layers and very shallow junctions, limiting light collection and sensitivity to higher wavelengths, respectively. In our case only a small number of pixels is necessary; they can be therefore made large and more traditional processes will suffice. The main advantages are predictable behavior, deeper photo-collecting junctions, availability and lower cost.

Either active- or passive-pixel architectures can be chosen. The first drives the pixel signal faster to the output and reduces readout noise, but requires node-voltage reset, besides introducing fixed-pattern noise (FPN), which on its turn requires correlated-double sampling (CDS) to suppress offset. On the other hand, the passive-pixel architecture introduces delay to the signal, but needs only the pixel-select control line and has virtually no FPN for large pixels, which is very convenient for zeroing of the spot position.

IV. Layout

The Hartmann mask was fabricated with sixty-four circular holes (ϕ = 450μm) located in an 8x8 orthogonal grid with a 1000μm pitch. It was placed 6 cm above the detector.

The detector consists of 256 pixels clustered four by four, so that an orthogonal array of 64 quad-cells (QC's) is formed. The chip has an integrated analog demultiplexer and a sampling-rate controller too, which allows random access to QC's and either 4 or 8 parallel outputs at a time. A diagram with the detector layout is shown in Figure 4.

There are two groups of QC's, those in the inner region and those in the outer region. Coupled and uncoupled operational modes are possible. In the first, every QC in the inner region is coupled to another one in the outer region, i.e., they are addressed simultaneously and 8 signals (4 from each QC) are sent to output terminals at a time. In this case a 5-bit address register is used. Conversely, in the uncoupled mode any QC in the whole chip is enabled by a 6-bit address and 4 signals are available at the output. Random QC addressing is possible in both modes. It gives the flexibility to, for instance, vary the number of amplifiers at the output and to zoom in a certain region of the array.

V. Implementation of the multi-spot position detector

A $1cm^2$ CMOS chip was implemented in a 1.6μm double-metal single-poly n-well process. Each QC consists of four 300μm x 300μm pixels (94% pixel fill factor), each with an attached switch set (Figure 5). Each pixel has two photodiode junctions: p^+/n-well and n-well/p^--epilayer (Figure 6). The photocurrent is read through an n^+ ohmic contact to the n-well. There is a 380μm gap between QC's so minimize interference between carriers generated by neighboring light spots.

A switch set is based on analog transmission gates that either transfer the photocurrent to the output bus or discharge the pixel. They have been designed with minimum-feature-size transistors, with charge attenuation and a digital inverter (Figure 7). The switch set takes 10μs to settle. The demultiplexer is split into several digital modules around the QC array, which control the analog data transmission at the on-pixel switch sets. The sampling-rate controller is an analog-switch batch that leads the digital control signals to a single QC region or to both regions.

VI. Performance

We used a He-Ne laser, λ = 0,633 μm, and the pixel quantum efficiency for this wavelength was found to be 40%. The sigmoidal response of a fabricated QC, for a 450μm 12μW spot is seen in Figure 8. The QC signal-to-noise ratio (SNR) depends basically on the intensity level and noise introduced by the amplification stage. Dark current is about 25nA at room temperature. When the spot centroid was confined to the central region of the detector and no data processing was made, we found that the SNR is 64 dB for a 12μW spot and 25dB for a 0.2μW spot, including amplification noise. The latter figure can be improved considerably if data is averaged, at the expense of operational speed. Position accuracy for spot displacements up to 100μm about the QC center is as low as 1.4μm, when SNR=64dB.

In the case of low-spatial-frequency aberrations, the best reconstruction is achieved with a small number of polynomial terms, once introduction of higher-order terms produces a noisy solution. High-spatial-frequency aberrations, however, require a larger number of terms and will be therefore reconstructed with lower accuracy. For 9 Zernike polynomials [5] and SNR=65dB, λ/20 RMS reconstruction accuracy is achieved. Pixel readout frequency is 100KHz and when the sampling-rate controller is set to the coupled mode, the frame rate is about 3 KHz. The overall system frequency, however, might be reduced due to data-acquisition time, data processing, reconstruction and eventually mirror control in close-loop.

VII. Conclusions

We fabricated a Hartmann wavefront sensor, with 256 pixels clustered as position-sensitive detectors. So far an analog demultiplexer, switch sets and sampling-rate controller have been included. The sensor can achieve λ/20 RMS reconstruction accuracy and features quad-cells with as low as 1.4μm position accuracy. It was designed to accommodate frame rates up to 3 KHz. If operated along with optimized computer algorithms and appropriate data-acquisition hardware, the overall operational frequency will be suitable for real-time applications.

VIII. Acknowledgements

From 1998 to 2000 the project was funded by TU-Delft. Since January 2001, sensor development has been supported by the Dutch Technology Foundation STW (project DOE 5375).

IX. References

[1] G. Love, "Adaptive Optics for Industry and Medicine'', World Scientific Publ. Co., 2000.

[2] J. Liang, D. Williams, D. Miller, "Supernormal Vision and High-resolution Retinal Imaging Through Adaptive Optics", J. Opt. Soc. Am., A14 (11), pp.2884-2892, 1997.

[3] D. Neal, T. O'Hern, J. Torczynski, M. Warren, R. Shul, T. McKechnie, "Wavefront Sensors for Optical Diagnostics in Fluid Mechanics", Proc. SPIE 2005, pp.194-200, 1993.

[4] D. W. de Lima Monteiro, G. Vdovin, P. Sarro, "Various layouts of analog CMOS optical position-sensitive detectors," Proc. SPIE, vol. 3794, pp.134-142, 1999.

[5] M. Born, E. Wolf, "The Principles of Optics", 7th edition, Cambridge University Press, 1999.

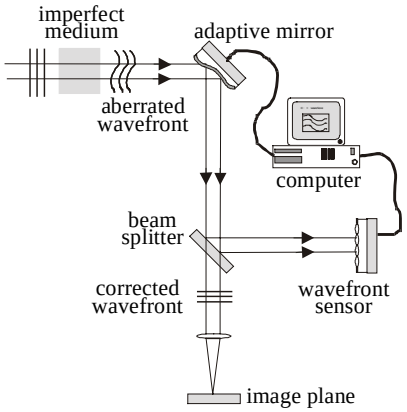

Fig. 1: Close-loop Adaptive Optics system

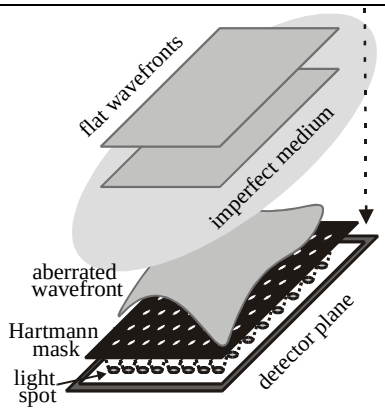

Fig. 2: Schematics of the Hartmann wavefront sensor

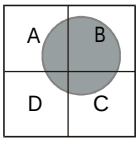

Fig. 3: Illustration of a quad-cell

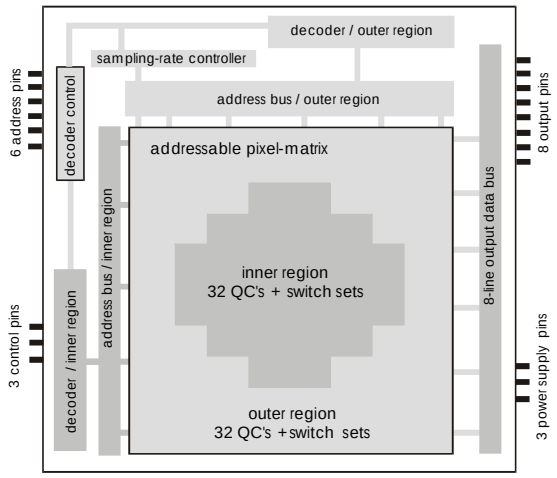

Fig. 4: Detector diagram

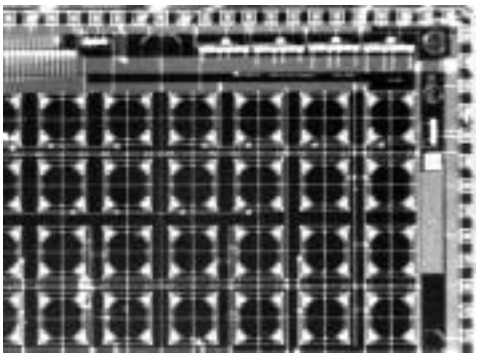

Fig. 5: Detail of implemented Hartmann sensor

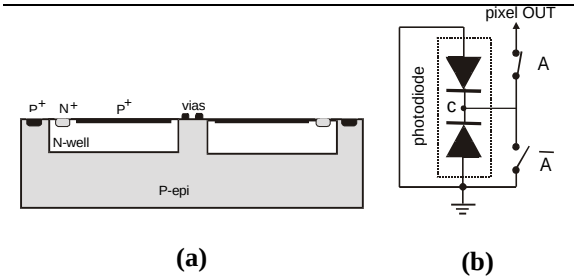

Fig. 6 – (a) Cross section of a QC. The vias are metal wires for internal contact, (b) pixel schematics.

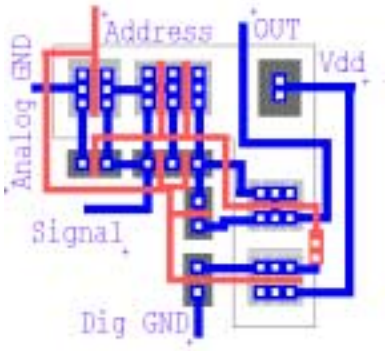

Fig. 7: Switch set layout, with inverter, transmission gates and charge attenuation.

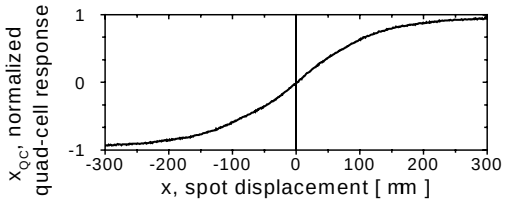

Fig. 8: Quad-cell response in x-direction for a 450μm 12μW spot.